

Reflectance Model for Quantifying Chlorophyll *a* in the Presence of Productivity Degradation Products

K. L. CARDER,¹ S. K. HAWES,¹ K. A. BAKER,² R. C. SMITH,³
R. G. STEWARD,¹ AND B. G. MITCHELL⁴

Marine colored dissolved organic matter (CDOM) (also gilvin or yellow substance) absorbs light at an exponentially decreasing rate as a function of wavelength. From 410 nm to about 640 nm, particulate phytoplankton degradation products including pheopigments, detritus, and bacteria have absorption curves that are similar in shape to that of CDOM. In coastal areas and areas downstream from upwelling regions, these constituents of seawater often absorb much more light than do living phytoplankton, leading to errors in satellite-derived chlorophyll estimates as high as 133%. Proposed NASA sensors for the 1990s will have spectral channels as low as 412 nm, permitting the development of algorithms that can separate the absorption effects of CDOM and other phytoplankton degradation products from those due to biologically viable pigments. A reflectance model has been developed to estimate chlorophyll *a* concentrations in the presence of CDOM, pheopigments, detritus, and bacteria. Nomograms and lookup tables have been generated to describe the effects of different mixtures of chlorophyll *a* and these degradation products on the $R(412) : R(443)$ and $R(443) : R(565)$ remote-sensing reflectance or irradiance reflectance ratios. These are used to simulate the accuracy of potential ocean color satellite algorithms, assuming that atmospheric effects have been removed. For the California Current upwelling and offshore regions, with chlorophyll *a* $\leq 1.3 \text{ mg m}^{-3}$, the average error for chlorophyll *a* retrievals derived from irradiance reflectance data for degradation product-rich areas was reduced from $\pm 61\%$ to $\pm 23\%$ by application of an algorithm using two reflectance ratios ($R(412) : R(443)$ and $R(443) : R(565)$) rather than the commonly used algorithm applying a single reflectance ratio ($R(443) : R(565)$).

1. INTRODUCTION

The next generation of ocean-viewing, visible/near-infrared satellite spectrometers will include for the first time a short-wavelength band which will permit improved chlorophyll *a* concentration determinations. The sea-viewing wide field-of-view sensor (SeaWiFS), the high-resolution imaging spectrometer (HIRIS), and the moderate-resolution imaging spectrometer (MODIS) planned for launch in the 1990s will all contain a wavelength band in the 410–420 nm range. On SeaWiFS, this band and a band at 490 nm will complement other bands (443, 520, 565, and 665 nm) that are similar to those of the coastal zone color scanner (CZCS). It will also have near infrared bands (765 and 865 nm) useful for separating water-leaving radiance from radiance scattered from atmospheric aerosols for coastal or other waters with high in-water backscattering.

Colored, dissolved organic matter (CDOM) (also gilvin or yellow substance), pheopigments, detritus, and associated bacteria (collectively referred to hereafter as “degradation products,” or DP) absorb more strongly in the 412-nm band than at longer wavelengths [see *Bricaud et al.*, 1981; *Kiefer and Soohoo*, 1982; *Kirk*, 1976, 1980, 1983; *Kishino et al.*, 1985; *Mitchell and Kiefer*, 1988a; *Roesler et al.*, 1989], whereas phytoplankton absorb more strongly at 443 nm than at 412 nm [*Jeffrey*, 1980; *Bricaud et al.*, 1983]. These

contrasting absorption characteristics can be exploited for the purpose of quantifying viable phytoplankton pigments (mainly chlorophyll *a* but including some accessory pigments) independently from DP. They also provide a means to remotely assess the absorption due to DP.

CZCS algorithms for estimating chlorophyll *a* (Chl *a*) plus pheophytin *a* (pheo *a*) concentrations perform quite well for regions of the ocean where scattering and absorbing components of seawater covary with these pigments [*Gordon and Morel*, 1983; *Gordon et al.*, 1983]. A number of empirical and semianalytical optical models have been developed to simulate the behavior of the underwater light field for such Morel case 1 waters [*Morel and Prieur*, 1977; *Smith and Baker*, 1978; *Baker and Smith*, 1982; *Gordon et al.*, 1988; *Morel*, 1988; *Mitchell and Holm-Hansen*, 1991; *Mitchell*, 1991]. Such models have been used as the basis for classifying water types and/or for developing remote sensing algorithms.

The accuracies of these models, however, may decrease when environmental conditions depart from those representative of the data set used to empirically derive the covariance relationships. For instance, DP including CDOM are produced when grazing, photolysis, and other mechanisms degrade the viable plant matter at and downstream from phytoplankton blooms. The DP-to-chlorophyll ratio will change dramatically for a parcel of upwelled water over a relatively short time, from chlorophyll-rich and DP-poor to DP-rich and chlorophyll-poor. Solid evidence for the occurrence of this scenario can be found in two separate studies. *Peacock et al.* [1988] found that absorption attributed to CDOM at 440 nm was at least sixteenfold that due to phytoplankton pigments within an offshore jet from an upwelling region, whereas pigments were the dominant absorption agents at the upwelling center near the coast. Similarly, *Carder et al.* [1989] found that particulate absorption at 440 nm decreased thirteenfold, while CDOM absorp-

¹Marine Science Department, University of South Florida, St. Petersburg.

²Marine Bio-Optics, Scripps Institution of Oceanography, University of California, San Diego, La Jolla.

³Center for Remote Sensing and Environmental Optics, University of California, Santa Barbara.

⁴Ocean Productivity Program, NASA, Washington, D. C.

Copyright 1991 by the American Geophysical Union.

tion at 440 nm increased by 60% in 10 days as they tracked a phytoplankton bloom from the Mississippi River plume to Cape San Blas. This widely varying CDOM-to-chlorophyll ratio has a profound effect on upwelled radiance in the blue 443-nm band of the CZCS and a smaller but still significant effect in the green 520-nm band. The correspondence in absorption at 443 nm and 520 nm between CDOM and chlorophyll creates erroneously high estimates of pigment concentration in those models which rely solely upon either of these spectral bands to indicate absorption due to phytoplankton.

Separate studies performed in the Southern California Bight point to another way to view the problem. *Smith and Baker* [1982] developed a pigment algorithm for that site that appears to require a larger absorption effect per unit of chlorophyll-like pigment than do most other case 1 algorithms [see *Gordon and Morel*, 1983]. However, the algorithm parameters for the Southern California Bight study region changed with time (compare *Smith and Baker* [1982] to *Smith and Wilson* [1981]), requiring contemporaneous ship and satellite data for parameter adjustment. *Mitchell and Kiefer* [1988a] found significant variability in pigment-specific particulate absorption in this region, which may account for some of the difference between the two algorithms, but the presence of CDOM and other degradation products can also cause such variation. In any event, without expensive surface verification, waters laden with DP cannot be unambiguously identified based upon satellite data from sensors using as limited a suite of spectral channels as the CZCS employed.

Another problem is that models which do not separate absorption due to viable pigments from absorption due to DP have less utility to researchers applying physiological primary production models that are driven by quanta absorbed by photosynthetic pigments [e.g., *Kiefer and Mitchell*, 1983; *Platt*, 1986; *Smith et al.*, 1989] or to researchers interested in the DP rather than the pigments.

A previously developed semianalytical reflectance model is modified here to address the concerns listed above. The model is used to develop an algorithm that utilizes a 412-nm spectral channel in addition to the 443-nm and 565-nm channels expected on SeaWiFS in order to estimate from irradiance reflectance data Chl *a* concentration and the absorption effects due to DP. In situ reflectance data from the California Current region is used to test the algorithm.

2. MODEL AND ALGORITHM DEVELOPMENT

Morel and Gordon [1980] describe three approaches to interpret ocean color data in terms of the in situ optical constituents: empirical, semiempirical, and analytical. In the analytical approach, (1) radiative transfer theory provides a relationship between upwelling irradiance and the in situ constituents, then (2) constituent concentrations are derived from irradiance values measured at several wavelengths by inversion of the resultant system of equations. The algorithm presented here uses this approach, and the term "semianalytical" is invoked because pieces of the radiative model are expressed by empirical relationships. This analytical derivation of the two quantities in question, Chl *a* and degradation products, avoids the problem of statistical nonvalidity, due to the spatial and spectral correlation between the two, that *Prieur and Sathyendranath* [1981] encountered in their at-

tempts to decouple the optical effects of those two quantities. In the following sections, the radiative transfer model will be developed, the individual terms in the resultant equations will be expressed in terms of Chl *a* and degradation product concentrations, and the algorithm for determining the constituent concentrations will be explained.

2.1. Reflectance Model

The concept of using spectral ratios of water-leaving radiance to determine phytoplankton pigment concentrations has enjoyed widespread currency ever since the idea first surfaced in the work by *Clarke et al.* [1970]. The most commonly applied algorithm for use with CZCS data corrected for atmospheric effects falls into the empirical category as described by *Morel and Gordon* [1980] and is described by

$$[C] = A(r_{ij})^B \quad (1)$$

where $[C] = [\text{Chl } a] + [\text{pheo } a]$ (square brackets here indicate concentration in mg m^{-3}), A and B are empirical constants, and r_{ij} is the spectral ratio of water-leaving radiance, defined as

$$r_{ij} = L_w(\lambda_i)/L_w(\lambda_j) \quad (2)$$

[*Gordon and Morel*, 1983]. Symbols not defined explicitly in the text can be found in the notation section.

Equation (2) derives from earlier research where r_{ij} represented $R(\lambda_i)/R(\lambda_j)$, the irradiance reflectance ratio. Irradiance reflectance is defined as

$$R(\lambda) = E_u(\lambda, 0-)/E_d(\lambda, 0-) \quad (3)$$

[*Morel and Prieur*, 1977], and a similar quantity, remote-sensing reflectance, is defined as

$$R_{rs}(\lambda) = \pi L_w(\lambda)/E_d(\lambda, 0+) \quad (4)$$

[see *Austin*, 1974; *Carder and Steward*, 1985], where $E_u(\lambda, 0-)$ is upwelling irradiance just below the sea surface and $E_d(\lambda, 0-)$ and $E_d(\lambda, 0+)$ are downwelling irradiances just below and just above the sea surface, respectively. The spectral ratio given by (2) can be expressed in terms of $R_{rs}(\lambda)$ as

$$r_{ij} = R_{rs}(\lambda_i)/R_{rs}(\lambda_j) * E_d(\lambda_i, 0+)/E_d(\lambda_j, 0+) \quad (5)$$

or, for areas where $E_u(\lambda, 0-)/L_w(\lambda)$ is only weakly dependent on wavelength [*Austin*, 1979], as the approximation

$$r_{ij} \approx R(\lambda_i)/R(\lambda_j) * E_d(\lambda_i, 0+)/E_d(\lambda_j, 0+) \quad (6)$$

since parameters associated with passing irradiance thru the air-sea interface are nonspectral. For cloudless skies, $E_d(\lambda, 0+)$ can be calculated based upon a number of models [*Justus and Paris*, 1985; *Bird and Riordan*, 1986; *Frouin et al.*, 1989; *Gregg and Carder*, 1990]. Thus reflectance data of either type can be used interchangeably in spectral ratio form as long as $E_u(\lambda, 0-)/L_w(\lambda)$ is relatively constant with wavelength. The implications of this condition will be considered in section 5.

Our model (called the "DP model") employs the spectral ratio concept but uses a semianalytical formulation of irradiance reflectance, $R(\lambda)$, rather than the empirical approach that is manifest in (1). Based upon the work of *Morel and*

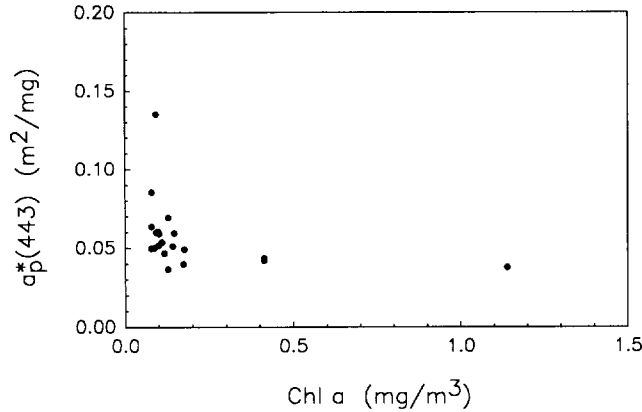


Fig. 1. Chl *a*-specific absorption coefficient at 443 nm for particles (including phytoplankton and PDP) versus [Chl *a*]. Data are from the fall 1982 ODEX cruise, near-surface ($z < 25$ m) samples only.

Priour [1977] and Gordon *et al.* [1975], $R(\lambda)$ can be expressed in terms of the inherent optical properties of the water:

$$R(\lambda) \approx 0.33(b'_w + b'_p)/(a_w + a_{\text{cdom}} + a_p) \quad (7)$$

where b' is the backscattering coefficient, a is the absorption coefficient, and the subscripts w , cdom , and p represent water, CDOM, and particles. The spectral dependence of each term has been left off for convenience. In practice, a_{cdom} corresponds to the fraction of a given water sample that passes through a 0.2- μm pore size filter, while a_p corresponds to the fraction that is retained on a Whatman GF/F glass-fiber filter. This approach ignores the absorption effects of bacteria and detritus in the size range of 0.2 to about 0.7 μm [Altabet, 1990].

A difficulty with the above expression is that absorption effects due to viable phytoplankton pigments, pheopigments, detritus, and bacteria are all a part of a_p . The last three of these components, referred to hereafter as "particulate degradation products" or PDP, do not contribute to the photosynthetic process, yet they often play a significant role in determining the magnitude of a_p , especially at the shorter wavelengths [Mitchell and Kiefer, 1988a]. This effect is apparent in Figure 1 where the Chl *a*-specific absorption coefficient for particles at 443 nm, $a_p^*(443)$, is graphed against [Chl *a*] for samples taken during the 1982 Optical Dynamics Experiment (ODEX) cruise off California. The variation in $a_p^*(443)$ is quite large, even over a small range of [Chl *a*] ($0.05 < [\text{Chl } a] < 0.2 \text{ mg/m}^3$). Although some of this variation may be due to the package effect (see section 2.4), evaluation of the absorption ratio $a_p(435) : a_p(675)$ yielded values as high as 7.08 with a mean value of 4.56, indicating that significant detrital absorption effects must also be present [see Mitchell and Kiefer, 1988a; Roesler *et al.*, 1989].

By removing the PDP absorption from a_p and regrouping it with the CDOM absorption term, an absorption coefficient that represents all DP, including the 0.2- to 0.7- μm size fraction, is formed ($a_{\text{dp}} = a_{\text{cdom}} + a_{\text{pdp}}$), as well as one which represents biologically utilizable absorption ($a_\phi = a_p - a_{\text{pdp}}$), assuming that all viable pigments are contained in

cells larger than the nominal GF/F pore size of 0.7 μm . This change leads to the following reformulation of (7):

$$R(\lambda) \approx 0.33(b'_w + b'_p)/(a_w + a_{\text{dp}} + a_\phi^*[\text{Chl } a]) \quad (8)$$

where a_ϕ^* is the Chl *a*-specific absorption coefficient due only to viable phytoplankton pigments. [Chl *a*] (used as a surrogate for the concentration of all photosynthetic pigments) is chosen as the index for specific absorption rather than the commonly used [Chl *a*] + [pheo *a*] since absorption due to pheopigments is included in the DP absorption term. As will be shown in section 2.3, this regrouping fits smoothly into the modeling scheme due to the similar spectral shapes of a_{cdom} and a_{pdp} .

Tables are available for both b'_w [Morel, 1974] and a_w [Smith and Baker, 1981]. Expressions for each remaining term in (8) will be developed for each of the three wavelengths 412, 443, and 565 nm. Two irradiance ratio equations will be formed from the three irradiance equations, forming the basis for the pigment and degradation product algorithm.

2.2. Spectral Backscattering Due to Particles

Expressions for b'_p at 443 nm and 565 nm are adapted from empirical formulas developed by Gordon *et al.* [1988]. They are

$$b'_p(443) = 0.0030[\text{Chl } a]^{0.22} \quad (9)$$

$$b'_p(565) = 0.0033[\text{Chl } a]^{0.36} \quad (10)$$

We have substituted [Chl *a*] for [*C*] and assumed that the backscattering coefficient at 565 nm is the same as that at 550 nm, the wavelength that is used by Gordon *et al.* [1988]. The spectral dependence of (9) and (10) is weak for the range of [Chl *a*] values encountered in this study ($[\text{Chl } a] \leq 1.3 \text{ mg m}^{-3}$; see Table 2), and particle backscattering will thus play only a minor role relative to absorption in affecting the spectral irradiance ratios. For waters where [Chl *a*] is of the order of 10 mg m^{-3} or larger, this may not be the case.

An expression for b'_p at 412 nm can be developed using arguments that parallel those of Gordon and Morel [1983] and Gordon *et al.* [1988]. We assume that (1) $b'_p(\lambda) = A(\lambda) [\text{Chl } a]^{B(\lambda)}$, where A and B are constants; (2) at high chlorophyll ($[\text{Chl } a] = 20 \text{ mg m}^{-3}$), $b'_p(412)/b'_p(443) = 1.2$ due to enhanced pigment absorption, and thus decreased backscattering, at 443 versus 412 nm; and (3) at low chlorophyll ($[\text{Chl } a] = 0.05 \text{ mg m}^{-3}$), backscattering follows a λ^{-1} power law [Gordon and Morel, 1983], yielding $b'_p(412)/b'_p(443) = 1.0752$. Applying the points in 2 and 3 to the equation in 1 leads to

$$b'_p(412)/b'_p(443) = 1.14[\text{Chl } a]^{0.016} \quad (11)$$

and substituting (9) yields

$$b'_p(412) = 0.0034[\text{Chl } a]^{0.24} \quad (12)$$

Different relationships are needed for situations where backscattering is poorly correlated with Chl *a*, within a coccolithophore bloom for example or where suspended sediments or other nonalgal scatterers are in high proportion to living cells.

2.3. Spectral Absorption by Degradation Products

Recently, the term CDOM has been employed to describe that fraction of the dissolved organic matter which modifies the color of the water by absorption of light (the terms gilvin, gelbstoff, or yellow substance are often used interchangeably with CDOM). The oceanographic and limnological literature is rife with reports of the absorption effects of CDOM [James and Birge, 1938; Jerlov, 1955; Kalle, 1961, 1966; Hojerslev, 1974; Stuermer, 1975; Lundgren, 1976; Kirk, 1976, 1980; Bricaud et al., 1981; Carder et al., 1989]. Similarly, PDP often has a significant effect on the spectral absorption of ocean particles, especially at short wavelengths [Kiefer and Soohoo, 1982; Kishino et al., 1985; Mitchell and Kiefer, 1988a; Roesler et al., 1989]. Both CDOM and PDP are accounted for in our degradation product absorption term.

In general, the CDOM found in most of the oceans of the world can be of either marine or terrigenous origin. However, G. Harvey (personal communication, 1991) has found that the molecular weights of the humic and fulvic acid samples collected from the euphotic zone of oceanic waters in several oceans and even in the offshore Mississippi River plume (salinity > 25‰) were less than 1000, indicative of a marine or aqueous rather than a terrigenous origin [Hayase and Tsubota, 1985; Carder et al., 1989]. This is important because the optical properties of marine humus are quite different from those of terrestrial humus. In addition, Carder et al. [1989] argue that at least for the Gulf of Mexico, CDOM absorption can largely be accounted for by the summed absorptions of marine humic acid (MHA) and marine fulvic acid (MFA). By adopting the approximation $a_{\text{cdom}} \approx a_h + a_f$, degradation product absorption can be expressed as

$$a_{\text{dp}} = a_h + a_f + a_{\text{pdp}} \quad (13)$$

where the subscripts *h* and *f* refer to MHA and MFA, respectively. Note that this approximation can only underestimate CDOM absorption.

Carder et al. [1989] have shown that spectral absorption curves for MHA and MFA can be fit by exponential functions of the form

$$a_x(\lambda) = C_x a_x^*(450) e^{S_x(450 - \lambda)} \quad (14)$$

where $a_x(\lambda)$ is the absorption coefficient of component *x* (*x* = *h* or *f*) at wavelength λ in m^{-1} , C_x is the concentration of *x* in g m^{-3} , $a_x^*(450)$ is the specific absorption coefficient of *x* at 450 nm in $\text{m}^2 \text{g}^{-1}$, and S_x is the spectral slope parameter of *x* in nm^{-1} . They determined that $a_h^*(450) = 0.1304 \text{ m}^2 \text{g}^{-1}$, $a_f^*(450) = 0.0073 \text{ m}^2 \text{g}^{-1}$, $S_h = 0.011 \text{ nm}^{-1}$, and $S_f = 0.019 \text{ nm}^{-1}$ for MHA and MFA samples from the Gulf of Mexico.

Furthermore, it is clear from the work of Kishino et al. [1985] and Roesler et al. [1989] that spectral absorption curves for PDP rather closely approximate the curve shapes for marine CDOM for wavelengths greater than 412 nm (see Figure 2). In fact, the global mean spectral slope for detrital absorption data (S_{pdp}) fit to an exponential curve like (14) was found by Roesler et al. [1989] to be 0.011 nm^{-1} . This value is the same as the spectral slope parameter S_h for MHA found by Carder et al. [1989], rendering the absorption by the two components spectrally inseparable. We thus

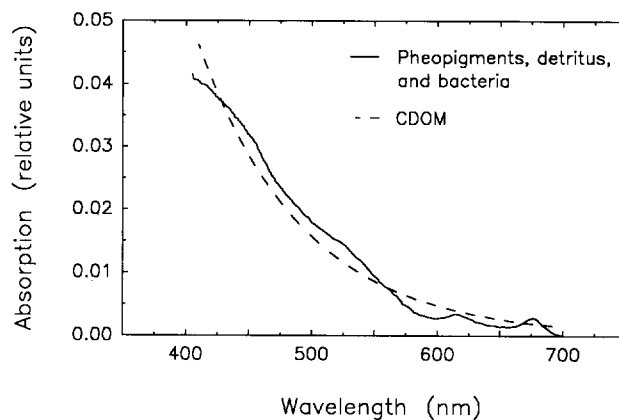


Fig. 2. Relative absorption coefficients versus wavelength for marine CDOM ($a_{\text{cdom}} \sim e^{0.014(450 - \lambda)}$) and PDP [from Kiefer and Soohoo, 1982].

define a weighted concentration parameter, C'_h , that accounts for both MHA and PDP in the same term:

$$C'_h = C_h + C_{\text{pdp}} a_{\text{pdp}}^*(450) / a_h^*(450) \quad (15)$$

The prime indicates that the parameter is not a true concentration, but one which includes PDP, which is weighted by the specific absorption coefficients.

Using (15) and the Gulf of Mexico parameters from Carder et al. [1989], (13) can be rewritten as

$$a_{\text{dp}} = 0.1304 C'_h e^{0.011(450 - \lambda)} + 0.0073 C_f e^{0.019(450 - \lambda)} \quad (16)$$

Here a_{dp} is a function of C'_h and C_f for a given wavelength. However, in order to apply an algorithm with two irradiance ratios, the model is underspecific unless a_{dp} can be parameterized in terms of just a single variable quantity (see section 2.5). This can be achieved by specifying a priori the MFA fraction of total DP. This fraction is defined as f' where

$$f' = C_f / C'_{\text{dp}} = C_f / (C'_h + C_f) \quad (17)$$

and C'_{dp} is called the "weighted degradation product concentration." Again, the prime is used to indicate that the weighted PDP concentration is present implicitly. The full equation for DP absorption is now

$$a_{\text{dp}} = C'_{\text{dp}} [0.1304(1 - f') e^{0.011(450 - \lambda)} + 0.0073 f' e^{0.019(450 - \lambda)}] \quad (18)$$

with C'_{dp} being the sole variable for a given f' and λ . Note that for regions where absorption due to CDOM is high relative to that due to PDP (which is usually the case), $C'_h = C_h$ and C'_{dp} is equivalent to the CDOM concentration.

It is important to remember that the parameters $a_h^*(450)$, $a_f^*(450)$, S_h , S_f , and f' , are not universal and that they should be evaluated on a site-specific basis. This is particularly important in regions that are heavily influenced by terrigenous and riverine CDOM, since the spectral slopes and especially the mass-specific absorption coefficients for humic and fulvic acids are dependent upon their molecular weights [Hayase and Tsubota, 1985; Carder et al., 1989], and since the molecular weights of soil-derived humus can exceed 100,000 [Hayase and Tsubota, 1985]. On the positive

side, *Mueller and Lange* [1989] have demonstrated that certain very large provinces exist which have stable or only slowly changing bio-optical parameters.

2.4. Spectral Absorption by Phytoplankton

In this section, expressions for the Chl *a*-specific absorption coefficient for phytoplankton, $a_{\phi}^*(\lambda)$, are developed as functions of [Chl *a*] for the three wavelengths of interest. This task is complicated by the complex bio-optical characteristics of phytoplankton. *Morel and Bricaud* [1981] showed theoretically that $a_{\phi}^*(\lambda)$ is a function of the absorption coefficient of the cell material, the intracellular pigment concentration, and cell size. The "pigment package" or self-shading effect that they describe results in an inverse relation between $a_{\phi}^*(\lambda)$ and cell size for a given internal cell pigment concentration and cell material absorption coefficient, and it is manifest most significantly near the pigment absorption maximum of 436 nm. Also, recent work has shown that $a_{\phi}^*(\lambda)$ varies with light [*Dubinsky et al.*, 1986; *Mitchell and Kiefer*, 1988b] and nutrient adaptation [*Sosik and Mitchell*, 1991]. These variations are due to the relative internal concentrations of Chl *a* and photoprotective pigments, and package effects. These lab studies suggest that $a_{\phi}^*(\lambda)$ for surface waters may also have a seasonal and latitudinal signature, dependent on species composition and light and nutrient history. In order to characterize phytoplankton absorption, a conceptual understanding is needed of how cell size, light history, and nutrient limitation affect the pigment packaging.

To begin, consider two studies that have pointed out the correlation between cell size and nutrient availability. *Herbland et al.* [1985] found that pigments in the submicron phytoplankton size fraction dominated pigment concentration values for oligotrophic surface waters in the equatorial Atlantic, whereas they were only a minor component for nutrient- and chlorophyll-rich waters near the bottom of the photic zone. *Carder et al.* [1986] found an analogous trend in the onshore-offshore direction for subtropical waters off Florida; that is, the pigments of the nutrient- and chlorophyll-rich inshore waters were generally found packaged in larger cells than were the pigments of the more oligotrophic offshore waters. These findings suggest that for a given light domain (e.g., season, latitude), [Chl *a*] is roughly correlated with ensemble average cell size, which in turn suggests a rough inverse correlation between [Chl *a*] and $a_{\phi}^*(\lambda)$.

Another factor to consider is that as [Chl *a*] approaches very low or high values, $a_{\phi}^*(\lambda)$ approaches physiological limits, rather like asymptotes. For decreasing [Chl *a*], the cell size and the package effect decrease until $a_{\phi}^*(\lambda)$ approaches the upper limit provided by soluble pigments which is about $0.10 \text{ m}^2 (\text{mg Chl } a)^{-1}$ at 435 nm for high-light, high-carotenoid conditions [*Bricaud et al.*, 1988]. For increasing [Chl *a*], $a_{\phi}^*(\lambda)$ decreases because a higher fraction of the pigments are contained in larger, pigment-rich cells in high-chlorophyll waters.

These two concepts, the inverse correlation between $a_{\phi}^*(\lambda)$ and [Chl *a*] and the fact that there are physiological upper and lower bounds on $a_{\phi}^*(\lambda)$ are used as the basis for a preliminary description of how $a_{\phi}^*(\lambda)$ may behave as a function of [Chl *a*]. We chose a hyperbolic tangent function to provide a curve shape that is limited by asymptotes, and logarithmic coordinates are used to deal with the large

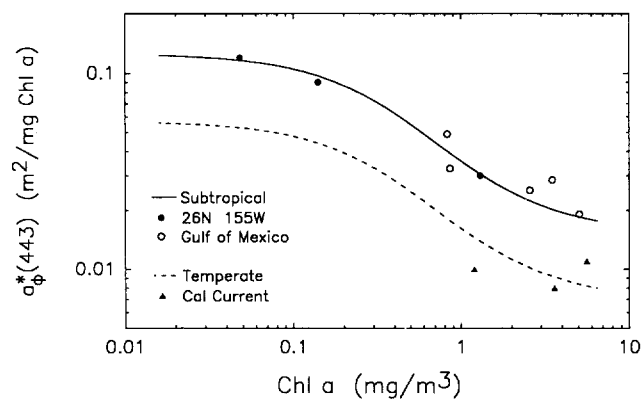


Fig. 3. Proposed functional relationships between Chl *a*-specific absorption coefficient at 443 nm for phytoplankton and [Chl *a*] for subtropical and temperate ocean regimes. Plotted points are "detritus-free" data that are available to corroborate the curves.

dynamic range of [Chl *a*] values found in natural waters (see Figure 3). For the 443-nm channel our expression has the generic form

$$a_{\phi}^*(443) = A \exp \{ B \tanh (C \ln ([\text{Chl } a]/D)) \} \quad (19)$$

where the parameters *A* and *D* describe the ordinate and abscissa of the point of symmetry for the curve, *B* describes the asymptotes of the graph, and *C* describes how quickly the curve approaches the asymptotes. Choosing values for the parameters *A*, *B*, *C*, and *D* requires that the curve be fit to an appropriate set of $a_{\phi}^*(443)$ versus [Chl *a*] data points. Since tropical and subtropical phytoplankton are typically smaller than are cells from temperate and boreal waters, a global empirical relationship would likely be less accurate due to package effects than would separate relationships for different oceanic regimes. Due to this size variation and to light history considerations, it makes sense to define at least two separate regimes, "subtropical" and "temperate."

Most of the phytoplankton absorption data used for adjusting the $a_{\phi}^*(443)$ versus [Chl *a*] curves for both regimes were determined by the simple and inexpensive GF/F filter pad transmission method described by *Mitchell and Kiefer* [1984, 1988b]. This method also incorporates absorption due to particulate detritus into the measured absorption spectrum, so only those data which are reasonably "detritus-free" have been used (a methodology for separating the absorption effects of phytoplankton from those due to detritus has been developed by *Kishino et al.* [1985], but unfortunately, few data using this methodology have been reported). Recently, *Stramski* [1990] reported that particulate optical densities determined by this method for two species of diatoms changed rapidly after filtration, presumably due to degradation of chlorophyll to pheopigments. However, a cyanobacterium and a flagellate species showed no such artifacts when tested, and it appears that absorption at 443 nm decreased by only about 8% 15 min after filtration of one of the diatom cultures. Since our samples are measured directly after filtration, the error introduced should be much smaller than 8%, especially if the phytoplankton assemblage on the filter pad is composed largely of species that do not exhibit the degradation effect.

The data sets for both regimes are sparse, but the subtropical data has a greater range of [Chl *a*] values, and it is

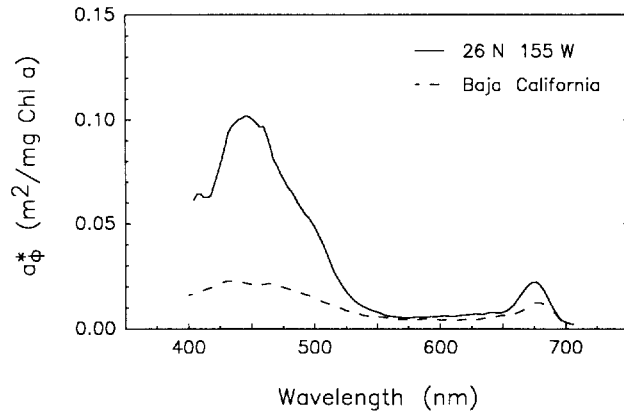


Fig. 4. Chl *a*-specific absorption coefficient for phytoplankton versus wavelength in a high light-adapted, oligotrophic environment (26°N, 155°W) and an eutrophic, coastal environment (Baja California). Picoplankton dominate the oligotrophic curve, where >65% of the Chl *a* passed through a 1.0- μ m Nuclepore filter. High-pressure liquid chromatography data for this station yielded relatively high ratios of carotenoid : Chl *a* [Laws *et al.*, 1990]. This helps to explain the high peak at about 440 nm with values >0.10 m² (mg Chl *a*)⁻¹. Additional factors causing this peak are the predominance of sub-micron cells, high light, and low nutrients, which typically result in low Chl *a* per cell. Detrital absorption effects have been removed from the eutrophic curve mathematically [Kiefer and Soohoo, 1982].

augmented on the high [Chl *a*] end by data for the Gulf of Mexico that has been derived from the work of Carder *et al.* [1986]. The subtropical data points consist of oligotrophic data from the spring bloom north of Hawaii and eutrophic data from near Baja California taken from Kiefer and Soohoo [1982], Laws *et al.* [1990], whose absorption data set is the one from which the oligotrophic data mentioned above derive, provide arguments for the detritus-free nature of those data, while detrital effects have been statistically removed from the Baja data. Figure 3 illustrates the proposed subtropical curve shape (as well as the proposed temperate curve), and it is described by

$$a_{\phi}^*(443) = 0.044 \cdot \exp \{1.05 \tanh (-0.60 \ln ([\text{Chl } a]/0.7))\} \quad (20)$$

While there is a need for additional data points to better corroborate the proposed curve shape, it does represent the data reasonably well.

The high-chlorophyll data points for the temperate curve in Figure 3 were determined via filter pad transmission from upwelling stations of the coastal transition zone cruise off northern California in July 1988. Only those data which exhibited relatively low particulate absorption at 400 nm relative to the absorption at 443 nm are used. Detritus-free data for low-chlorophyll temperate waters have not been located however, precluding an attempt to empirically adjust the equation parameters. In light of the limited data available, we have adopted the subtropical curve shape and adjusted the lead coefficient downwards from 0.044 to 0.02 in order to provide a temperate relationship for algorithm development purposes. Note that the curve does appear to provide a general lower limit to the ODEX specific absorption data shown in Figure 1. It is this temperate regime expression that is used in the reflectance model.

The curves in Figure 4 are used to develop package-effect

relationships that express $a_{\phi}^*(412)$ and $a_{\phi}^*(565)$ as fractions of $a_{\phi}^*(443)$. The $a_{\phi}^*(\lambda)$ curve from a high-light, oligotrophic, subtropical environment where picoplankton predominate was obtained at 26°N, 155°W at a depth of 20 m on April 2, 1987. This curve was measured via the filter pad transmission method of Mitchell and Kiefer [1984, 1988b], and it has a minimal package effect. The $a_{\phi}^*(\lambda)$ curve for high-chlorophyll subtropical waters is the ensemble-average curve of Kiefer and Soohoo [1982] for coastal waters near Baja California with the detrital absorption effects statistically removed. Once again the hyperbolic tangent function in logarithmic coordinates was chosen to model these relationships. Using points from Figure 4 to determine extrema yielded the following expressions:

$$a_{\phi}^*(412) = \{0.85 \exp \{0.2 \tanh (0.4 \ln ([\text{Chl } a]/.6))\}\} a_{\phi}^*(443) \quad (21)$$

$$a_{\phi}^*(565) = \{0.2 \exp \{0.4 \tanh (0.4 \ln ([\text{Chl } a]/.6))\}\} a_{\phi}^*(443) \quad (22)$$

It must be emphasized that by no means are the formulations developed in this section meant to be universal. The generic forms are used in an attempt to model the behavior of $a_{\phi}^*(\lambda)$ as a function of [Chl *a*] based on the theoretical concepts regarding the package effect discussed earlier. In light of the limited data available, the relationships given are first approximations that can be tolerated temporarily in order to develop the algorithm as a whole. As data sets of adequate size emerge, the new relationships that result can easily be inserted into the model. Researchers are encouraged to develop $a_{\phi}^*(\lambda)$ expressions for various environments using the improved qualitative filter technique of Mitchell [1990], augmented by both detrital correction [Kishino *et al.*, 1985] and pheopigment absorption correction [Roesler *et al.*, 1989].

2.5. Pigment Algorithm

Inserting the appropriate expressions for each of the terms in the irradiance reflectance equations (equation (8) with $\lambda = 412, 443, \text{ and } 565 \text{ nm}$) results in the two irradiance reflectance ratios

$$\frac{R(412)}{R(443)} = \frac{[b'_w(412) + b'_p(412)][a_w(443) + a_{dp}(443) + a_{\phi}(443)]}{[b'_w(443) + b'_p(443)][a_w(412) + a_{dp}(412) + a_{\phi}(412)]} \quad (23)$$

$$\frac{R(443)}{R(565)} = \frac{[b'_w(443) + b'_p(443)][a_w(565) + a_{dp}(565) + a_{\phi}(565)]}{[b'_w(565) + b'_p(565)][a_w(443) + a_{dp}(443) + a_{\phi}(443)]} \quad (24)$$

where

$$a_{dp}(\lambda) = [0.1304(1 - f')e^{0.011(450 - \lambda)} + 0.0073f'e^{0.019(450 - \lambda)}]C'_{dp}$$

$$a_{\phi}(412) = 0.85e^{0.2 \tanh\{0.4 \ln([\text{Chl } a]/0.6)\}}a_{\phi}(443)$$

$$a_{\phi}(443) = 0.02e^{1.05 \tanh\{-0.6 \ln([\text{Chl } a]/0.7)\}}[\text{Chl } a]$$

$$a_{\phi}(565) = 0.20e^{0.4 \tanh\{0.4 \ln([\text{Chl } a]/0.6)\}}a_{\phi}(443)$$

By forming two irradiance reflectance ratios, $R(412)/R(443)$ and $R(443)/R(565)$, we have two equations written in two unknowns, $[\text{Chl } a]$ and C'_{dp} . Since analytical inversion of this system of equations is difficult, nomograms (Figure 5) and computer look-up tables are generated that relate paired values of $R(412)/R(443)$ and $\log[R(443)/R(565)]$ to varying paired values of $[\text{Chl } a]$ and C'_{dp} for a given fulvic acid fraction f' . The right sides of (23) and (24) are solved for a two-dimensional array of $[\text{Chl } a]$ and C'_{dp} values at a fixed f' and the corresponding array of irradiance reflectance ratios is tabulated in Table 1. Forty-six discrete concentration values for each ocean color constituent were used to construct the look-up tables, ranging from 0.01 to 3.0 mg m^{-3} for $[\text{Chl } a]$ and from 0 to 6.0 g m^{-3} for C'_{dp} . Three look-up tables were constructed, corresponding to fulvic acid fractions of 0.89, 0.92, and 0.95. Irradiance reflectance ratio data can be compared to the calculated values in the look-up tables, and estimates of $[\text{Chl } a]$ and C'_{dp} can be obtained via two-dimensional linear interpolation of the input spectral ratios between the tabulated spectral ratios. Quick estimates can be made by selecting points on the nomogram (Figure 5).

3. FIELD MEASUREMENTS

The optical field measurements used to test this algorithm (referred to as the "DP algorithm") consist of irradiance reflectance measurements taken in the top attenuation layer ($z < 1/k_d(490 \text{ nm})$) during the fall 1982 ODEX cruise west of California (see Figure 6 for station locations). The environment included oligotrophic, coastal transition, and eutrophic water types. Measurements of $E_u(\lambda)$ and $E_d(\lambda)$ were made using the Biospherical Instruments Bio-Optical Profiling System (BOPS, described by *Smith et al.* [1984]) for λ

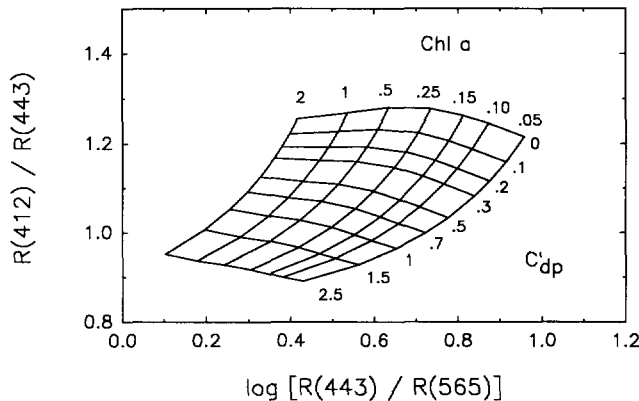


Fig. 5. Nomogram of $[\text{Chl } a]$ (mg m^{-3}) and C'_{dp} (g m^{-3}) as a function of $R(412)/R(443)$ and $\log[R(443)/R(565)]$. $C'_{dp} = C_h + C_f + C_{pdp} a_{pdp}^*(450)/a_h^*(450)$. Here, $f' = 0.92$.

TABLE 1. Summary of the Individual Scattering and Absorption Curves

	λ		
	412	443	565
$b_w(\lambda)$	0.00333	0.00237	0.000872
$b_p(\lambda)$	0.0034 $[\text{Chl } a]^{0.24}$	0.0030 $[\text{Chl } a]^{0.22}$	0.0033 $[\text{Chl } a]^{0.36}$
$a_w(\lambda)$	0.0160	0.0145	0.0787

= 410, 441, 465, 488, 520, 540, 560, 589, 625, 671, 694, and 767 nm. To minimize the effect of changing skies [*Smith and Baker, 1984*] and ship shadow effects [*Gordon, 1985; Smith and Baker, 1986*], we only used measurements that were taken on sunny days, simulating conditions appropriate for remote sensing. The BOPS wavelengths 410, 441, and 560 nm are used as surrogates for the DP model wavelengths of 412, 443, and 565 nm, which are the proposed wavelengths for Sea-WiFS. The appropriate measured irradiance reflectance ratios are given in Table 2.

$[\text{Chl } a]$ values are based on in situ fluorescence measured at 10 m depth. Discrete chlorophyll and pheopigment determinations were made at selected depths on each cast using a Turner 111A fluorometer. Millipore HA filters of pore size 0.45 μm were used to filter each seawater sample. These filters dissolve in 90% acetone which permits a no-grind chlorophyll extraction technique [*Smith et al., 1981*]. The BOPS provided measurements of continuous vertical pigment fluorescence which were then calibrated by the discrete extracted chlorophyll values available for each cast.

4. RESULTS

The optical data set described above has been used for input to both the DP algorithm and to an appropriate Case 1 algorithm. First, $R(\lambda)$ is calculated from $E_u(\lambda)/E_d(\lambda)$ for $\lambda = 412, 443, \text{ and } 565 \text{ nm}$. For the DP algorithm, $[\text{Chl } a]$ and

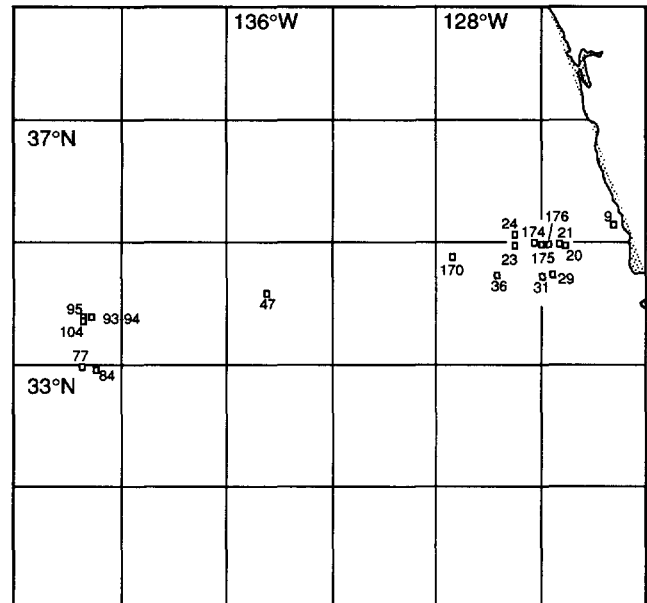


Fig. 6. Station locations for ODEX cruise, fall 1982.

TABLE 2. Measured and Modeled [Chl *a*] Values From ODEX Cruise, Fall 1982

Station	$R(410)$	$R(441)$	Chl <i>a</i> (Measured)	pheo <i>a</i> (Measured)	C (Case1)	Chl <i>a</i> (DP)	C'_{dp} (DP)	C'_{dp} Chl <i>a</i>
	$R(441)$	$R(560)$						
9d	0.922	1.116	1.307	0.42	1.400	1.909	3.355	2.57
9u	0.903	1.129	1.311	0.42	1.372	1.337	3.846	2.93
21d	0.965	2.877	0.130	0.06	0.250	0.191	1.419	10.91
21u	0.926	2.839	0.121	0.05	0.256	0.109	1.831	15.13
23d	0.988	3.973	0.128	0.04	0.139	0.104	0.959	7.49
23u	1.007	4.247	0.128	0.04	0.123	0.106	0.808	6.31
24d	0.987	4.263	0.112	0.03	0.122	0.084	0.911	8.13
29d	0.917	2.156	0.242	0.10	0.423	0.201	2.390	9.87
30d	0.992	3.492	0.136	0.05	0.176	0.152	1.046	7.69
30u	0.998	3.520	0.139	0.05	0.173	0.161	1.000	7.19
36d	1.020	4.295	0.122	0.04	0.121	0.116	0.741	6.07
47d	1.102	6.029	0.085	0.01	0.065	0.088	0.303	3.56
77.1d	1.109	6.522	0.074	0.03	0.056	0.074	0.259	3.50
77.2d	1.173	6.659	0.074	0.03	0.054	0.099	0.130	1.76
84u	1.142	6.328	0.102	0.06	0.060	0.097	0.200	1.96
93u	1.101	6.087	0.091	0.09	0.064	0.085	0.303	3.33
94d	1.141	5.999	0.105	0.08	0.066	0.111	0.221	2.10
95d	1.097	6.135	0.113	0.02	0.063	0.081	0.309	2.73
104u	1.131	6.142	0.108	0.01	0.063	0.099	0.234	2.16
170.2d	1.045	4.317	0.140	0.04	0.119	0.141	0.637	4.54
170.2u	1.046	4.374	0.142	0.04	0.117	0.138	0.624	4.39
174d	0.937	3.327	0.158	0.04	0.192	0.084	1.508	9.54
175.1d	0.946	2.963	0.253	0.00	0.237	0.135	1.564	6.18
176.1d	0.901	1.825	0.308	0.11	0.572	0.238	3.010	9.77
176.1u	0.897	1.860	0.299	0.11	0.553	0.202	3.084	10.31
176.2d	0.900	1.589	0.328	0.12	0.736	0.360	3.329	10.15

From left to right the columns represent the ODEX station number, measured irradiance reflectance ratios, measured [Chl *a*] and [pheo *a*], [C] calculated with the case 1 algorithm, [Chl *a*] and C'_{dp} calculated with the DP algorithm, and the ratio of (modeled C'_{dp}): (measured Chl *a*). [Chl *a*] and [pheo *a*] are in mg m^{-3} and C'_{dp} is approximately equal to CDOM concentration in g m^{-3} .

C'_{dp} are calculated from $R(\lambda)$ values as described in section 2.5, and for the case 1 algorithm, [C] is calculated by

$$[C] = 1.71[R(440)/R(560)]^{-1.82} \quad (25)$$

which is described in further detail by *Gordon and Morel* [1983]. [Chl *a*] estimated from the DP algorithm and [C] derived from the Case 1 algorithm are compared with measured [Chl *a*], and the performance of the two algorithms are tested. Only the accuracy of the Chl *a* portion of the DP algorithm could be tested since measurements of DP absorption are unavailable for comparison with the model estimates of C'_{dp} . The results are given in Table 2.

Before employing the DP algorithm it is necessary to specify f' , the fulvic acid fraction of total CDOM. The DP algorithm was run three times with f' held constant for each run at values of 0.89, 0.92, and 0.95. The total average error in calculated [Chl *a*] versus measured [Chl *a*] was the lowest for $f' = 0.92$, and it is assumed that 0.92 is the "regional average" f' . It is the results from this run that are shown in Table 2. Used in this manner, the DP algorithm cannot be purely predictive without some prior knowledge of f' . Fortunately, as will be seen in section 5, this problem should not be large.

The results are depicted graphically in Figure 7. Figure 7a shows [Chl *a*] derived from the DP algorithm and [C] derived from the case 1 algorithm versus measured [Chl *a*] for all 26 stations. High Chl *a* points ([Chl *a*] > 1) are well described by the case 1 algorithm, whereas the DP algorithm estimates are less accurate. Two observations may help to explain this. First, Table 2 reveals that the ratio (modeled C'_{dp}):(measured [Chl *a*]) is relatively low for these waters,

indicating that pigment absorption is the dominant influence on the $R(443) : R(565)$ reflectance ratio; the case 1 algorithm works well when noncovarying optical components (e.g., CDOM) are not high. Second, the nomogram (Figure 5) shows that the DP algorithm becomes increasingly sensitive to changes in the input reflectance ratios at higher Chl *a* and C'_{dp} . Thus the DP algorithm will be less accurate at high Chl *a* than in regions of medium-to-low Chl *a* ([Chl *a*] < 1).

Figure 7b is the same as Figure 7a except that only the medium-to-low Chl *a* points are plotted. At this greater resolution the case 1 algorithm can be characterized by two distinct regions: a low Chl *a* region in which [Chl *a*] estimates are consistently lower than the measured values and a medium Chl *a* region in which they are consistently higher than the measured values. The DP algorithm predicts [Chl *a*] more accurately in these regions, showing little or no net bias at low chlorophyll and only a slight low bias in the medium region.

Another way to present these data is to plot the percent error in [Chl *a*] estimates for the two methods versus the $C'_{dp} : [\text{Chl } a]$ ratio (see Figure 8). The mean fractional error for all stations was $\pm 38\%$ for the case 1 algorithm and $\pm 18\%$ for the DP model. The highest errors, up to 133%, occur in using the case 1 model for waters with the highest $C'_{dp} : [\text{Chl } a]$.

The percent error for the case 1 algorithm in Figure 8 correlates well with the $C'_{dp} : [\text{Chl } a]$ ratio, suggesting that this ratio can be used to indicate which waters are well described by the case 1 algorithm and which waters are not. For this particular cruise at least, an operational means of establishing the boundaries between true case 1 and DP-rich

waters is to designate the case 1 waters as those for which $C'_{dp} : [Chl a] < 7 \text{ g mg}^{-1}$. Waters with high C'_{dp} values are not necessarily DP-rich by this definition, notably stations 9d and 9u. Subdividing the study area in such a way is consistent with the concept of "bio-optical provinces" [Platt and Sathyendranath, 1988; Mueller and Lange, 1989], which states that the absorption and scattering properties of seawater vary from one geographical region to the next and with respect to time (e.g., seasonal variation).

Referring to the station location map (Figure 6) and to the tabulated $C'_{dp} : [Chl a]$ values (Table 2), it can be seen that in general, the DP-rich waters are found seaward of station 9 and landward of station 36. Thus both the pigment-rich coastal upwelling waters (represented here solely by station 9) and those waters found beyond the coastal transition waters more than 400 km offshore are case 1 waters using this criterion, while those found in the transition waters between the coastal and offshore waters are DP-rich. The only exceptions to this geographic scheme are stations 23u and 175.1d, which are within the oceanographic DP-rich boundaries but which barely miss the DP-rich criteria. Given the rather chaotic nature of currents off the west coast of California [see Abbott et al., 1990], this is well within the scope of expected patchiness. Also, the application of this

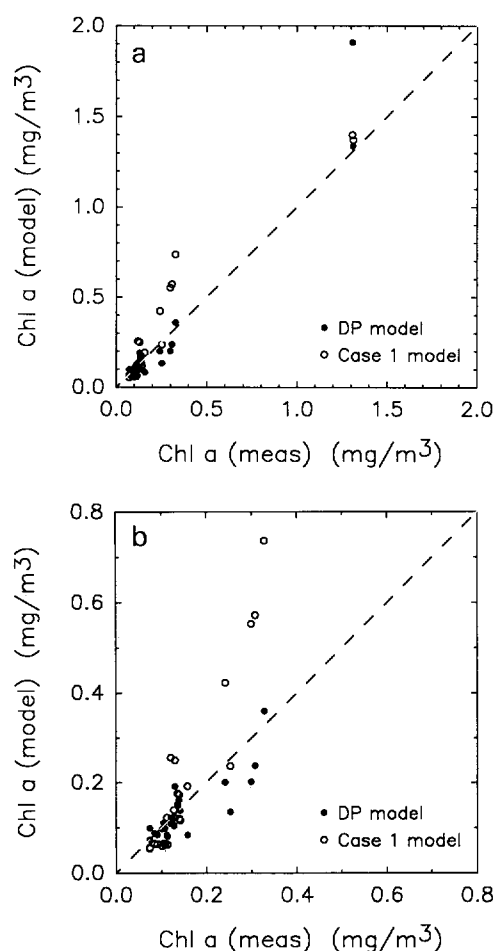


Fig. 7. Plot of [Chl *a*] derived from the DP model and [C] derived from the case 1 model ($[C] = 1.71 [R(440)/R(560)]^{-1.82}$) versus measured [Chl *a*]. Figure 7a includes all data points, while Figure 7b is a magnification of the lower concentration range. The dashed line is the 1:1 slope line.

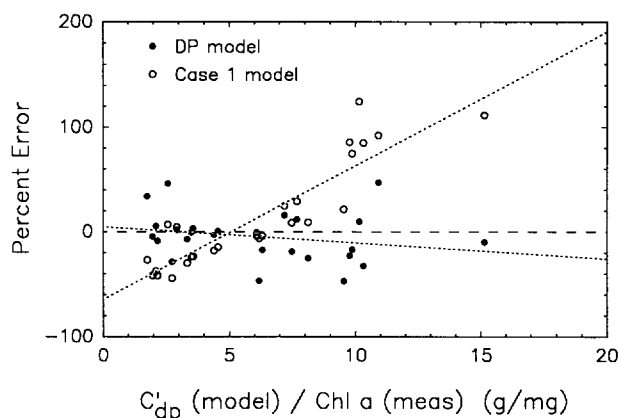


Fig. 8. Percent error ($= (\text{modeled } [Chl a] / \text{measured } [Chl a]) - 1 \times 100$) for the DP model and the case 1 model as a function of the ratio of modeled C'_{dp} to measured [Chl *a*]. The long dashed line is the zero line. The short dashed lines are linear regression lines for the two data sets: $Y = -1.53X + 4.88 (r^2 = 0.05, n = 26)$ for the DP model data, and $Y = 12.8X - 64.7 (r^2 = 0.80, n = 26)$ for the case 1 model data.

criterion depends on the estimated value of C'_{dp} , introducing another modicum of imprecision.

For the 11 DP-rich stations, the mean error using the case 1 algorithm for [Chl *a*] was $\pm 61\%$, while that for the DP algorithm was $\pm 23\%$. The net positive bias in the case 1 estimates for these waters will yield a corresponding inflation of any primary productivity estimates that are based on such values, while the DP algorithm provided only a slight negative bias for these same waters. For the case 1 waters (15 stations) the case 1 algorithm had a mean fractional error of $\pm 22\%$ with a net negative bias and the DP algorithm had $\pm 14\%$ error with little or no net bias. The error percentages are summarized in Table 3.

5. DISCUSSION

5.1. Comparison of the DP Algorithm Versus the Case 1 Algorithm

The most significant result of this study is the considerable improvement in [Chl *a*] retrieval accuracy of the DP algorithm over the case 1 algorithm (23% error versus 61% error) for those waters which our model estimates to be DP-rich and where $[Chl a] \leq 1.3 \text{ mg m}^{-3}$. Although the case 1 algorithm estimates [C], the sum of [Chl *a*], and [pheo *a*], Table 2 demonstrates that [C] and [Chl *a*] differ by only 10–40% and the presence of [pheo *a*] can only explain a minor fraction of the case 1 [Chl *a*] error for the DP-rich

TABLE 3. Mean Fractional Error in [Chl *a*] Estimates for Both Case 1 and DP Algorithms

Data Subset	Algorithm, %		
	Case 1	DP	<i>n</i>
All stations	38	18	26
$C'_{dp} : [Chl a] < 7 \text{ g mg}^{-3}$	22	14	15
$C'_{dp} : [Chl a] > 7 \text{ g mg}^{-3}$	61	23	11

Percent error is $[(\text{modeled } [Chl a]) / (\text{measured } [Chl a]) - 1] \times 100$. *n* is number of stations.

stations. Some other color constituent must be causing the large overestimates of [Chl *a*] generated by the case 1 algorithm presented here. Since there is no significant source of riverine or terrestrial CDOM in our study area and since detrital particles are likely to settle out quickly (as *Abbott et al.* [1990] found off northern California), marine CDOM is the only reasonable component of the DP ensemble that remains to explain the optical effects that we observe. This interpretation contradicts the assertions that marine CDOM always covaries with algal pigments or that its measurable influence is everywhere weak [*Morel and Prieur*, 1977; *Bricaud et al.*, 1981; *Gordon and Morel*, 1983]. These assertions are further undermined by two previously mentioned studies in which absorption due to CDOM increased with time in the same water mass (*Peacock et al.* [1988] and *Carder et al.* [1989]; see section 1).

In addition, [Chl *a*] estimates from the DP algorithm are better suited for use with primary productivity models than are those of the case 1 algorithm. First, [Chl *a*] estimates from the DP algorithm are relatively free of bias with respect to the measured values, whereas [C] estimates from the case 1 algorithm have considerable high bias in the DP-rich areas of the study region and low bias in the case 1 areas (see Figure 8). These biases will lead to systematic regional errors in primary productivity estimates. Second, primary productivity models that are based on physiological considerations need to be driven by photon absorption by viable pigments. The DP algorithm explicitly estimates [Chl *a*], the major photosynthetic pigment, whereas the pigment estimates of the various case 1 algorithms (including *Gordon and Morel* [1983], *Gordon et al.* [1988], and *Morel* [1988]) inherently include pheopigments and other degradation products which do not contribute to the photosynthetic process.

5.2. Regression Analyses

The regression analyses performed on the data depicted in Figure 8 indicate that 80% of the variance in error values for the case 1 [Chl *a*] algorithm could be accounted for by changes in the $C'_{dp}:[\text{Chl } a]$ ratio, while only 5% of the variance in error values for the DP [Chl *a*] algorithm error could be so explained. Caution must be used in interpreting these results, not only because the C'_{dp} values are estimates and not actual measurements but also because their values are inherently linked to the DP algorithm [Chl *a*] values with which they are being compared. *Prieur and Sathyendranath* [1981] used ridge regression to overcome this problem of correlation between independent variables. Since our only concern here is that the covariance between the case 1 error and $C'_{dp}:[\text{Chl } a]$ appears to be high, suggesting that a non-case 1, site-specific [Chl *a*] algorithm of the type described by equation (1) (i.e., a CZCS-type algorithm) can be developed, the correlation problem was not investigated further. A linear regression of $\log(\text{measured } [\text{Chl } a])$ versus $\log(R(440)/R(560))$ ($r^2 = 0.84$, $n = 26$) results in the following "case 1 + case 2" algorithm:

$$[\text{Chl } a] = 0.80[R(440)/R(560)]^{-1.26} \quad (26)$$

In comparison, *Morel* [1980] describes a similar "case 1 + case 2" reflectance ratio algorithm, given by

$$[C] = 1.62[R(440)/R(560)]^{-1.40} \quad (27)$$

($r^2 = 0.76$, $n \approx 90$; see *Gordon and Morel* [1983] for more details), which has a similar slope but a lead coefficient which is twice as large as the algorithm for the data in this paper. This difference can be accounted for in part by the fact that *Morel's* algorithm is for [C], which contains pheopigments, whereas the ODEX data do not, and that *Morel's* data set includes largely tropical and subtropical data where there are likely larger Chl *a*-specific absorption coefficients at 440 nm than there are for the more temperate ODEX data (see Figure 3). The algorithm expressed by (26) provides a means to estimate the viable pigments for the low-light, late fall time period in the ODEX region using a CZCS-type algorithm.

5.3. Variability of f'

The results of the DP algorithm assume that $f' = 0.92$, and some of the error in our DP model results may be explainable in terms of a variable f' . However, iterative trials of the DP algorithm in which f' was allowed to vary by ± 0.03 about the "regional average" of 0.92 for each station yielded little or no improvement in the mean fractional error for [Chl *a*] estimates, so using a single value of f' for the entire study region is probably not a bad approximation.

However, on a larger spatial scale, f' varies significantly. *Carder et al.* [1989] evaluated the spectral slope values of *Bricaud et al.* [1981] in terms of MHA and MFA absorption and found that their global average value ($S = 0.014 \text{ nm}^{-1}$ from 370 nm to 440 nm) was consistent with an f' value of 0.89. Similarly, the spectral slope for the western north Atlantic data of *Topliss et al.* [1989] ($S = 0.013 \text{ nm}^{-1}$) is consistent with an f' value of 0.84. Analyzing 11 published values of f' taken from the Gulf of Mexico [*Harvey et al.*, 1983; *Carder et al.*, 1989] yields a mean of 0.878 and a sample standard deviation of 0.098. This exercise indicates that selection of an appropriate mean value of f' for use in the DP model is site-dependent. For river plumes and areas heavily influenced by terrestrial runoff, the entire a_{dp} term needs reassessment, since the geochemistry of CDOM is different for terrestrial and riverine versus marine ecosystems, resulting in significant variation in the humic/fulvic ratio, the mass-specific absorption coefficients, and the CDOM molecular weights.

5.4. DOC Estimate

The concentration parameter C'_{dp} can provide a rough measure of dissolved organic carbon (DOC) if the factors in the following equation can be estimated:

$$\text{DOC} = C'_{dp} \frac{(C_h + C_f)}{C'_{dp}} \frac{\text{DOC}_{uv}}{(C_h + C_f)} \frac{\text{DOC}_{pt}}{\text{DOC}_{uv}} \quad (28)$$

where DOC_{uv} is the total DOC measurable by the ultraviolet oxidation technique [*Armstrong et al.*, 1966] and DOC_{pt} is the total DOC measurable by the new platinum-catalyst method [*Sukuki et al.*, 1985; *Sugimura and Suzuki*, 1988]. The factor $(C_h + C_f)/C'_{dp}$ corrects C'_{dp} for PDP and can be approximated by the easily measurable ratio $a_{cdom}(410)/a_{dp}(410)$. The factor $\text{DOC}_{uv}/(C_h + C_f)$ adjusts for the fact that DOC does not consist only of humic and fulvic acids, and the final factor provides a correction for the platinum-catalyst method versus the older ultraviolet technique. A $\text{DOC}_{uv}/(C_h + C_f)$ value of about 3.5 is provided by *Harvey*

et al. [1983] for both oligotrophic waters ($z = 20$ m), and for a low-chlorophyll, high-CDOM (i.e., DP-rich) station, both in the Gulf of Mexico. *Druffel et al.* [1989] found that the platinum-catalyst method and the UV oxidation technique yielded DOC values of about 210 and 90 mg at DOC m^{-3} , respectively, in the top 100 m at 31°N, 159°W, which provides a $\text{DOC}_{\text{pt}}/\text{DOC}_{\text{uv}}$ ratio of 2.3. If $(C_h + C_f)/C'_{\text{dp}}$ is near 1.0, these factors yield a mean estimated DOC concentration of 1.93 g DOC m^{-3} for the cluster of seven oligotrophic stations in this study that are west of 140°W and near 33°–34°N. Using these same factors, the 12 DP-rich stations in this study have a mean estimated DOC concentration of 14.8 g DOC m^{-3} . The oligotrophic ODEX data and the *Druffel et al.* [1989] data mentioned above are both taken from the North Pacific gyre, so the proximity of our estimate (1.93 g DOC m^{-3}) to those of *Druffel et al.* [1989] (2.52 g DOC m^{-3}) is reassuring. However, the steps between the modeled C'_{dp} and derived DOC estimates contain general approximations that have not been tested at the study site. Care in interpreting C'_{dp} in terms of DOC should be exercised at all study sites, especially those in coastal waters where $\text{DOC}_{\text{uv}}/(C_h + C_f)$ ratios can be quite variable [see *Harvey et al.*, 1983].

5.5. Optical Effects on Water-Leaving Radiance

The DP model presented here is based on irradiance reflectance and is thus well-suited for use with moored or free-floating buoys with instrumentation located at 5–10 m depth (depths typical of the data set utilized in this study). However, in judging the applicability of this model for use with water-leaving radiance data, additional concerns must be addressed. In making the transition from upwelling irradiance, $E_u(\lambda, 10 \text{ m})$, to water-leaving radiance, $L_w(\lambda)$, consideration must be given to changes in $R(\lambda)$ with depth, spectral variations in $E_u(\lambda, 0-)/L_u(\lambda, 0-)$, and transpectral effects due to water Raman scattering and solar stimulated fluorescence from CDOM.

Monte Carlo simulations by *Kirk* [1984] show that $R(\lambda)$ changes very little with depth for inelastic scattering, so this effect should be negligible. However, although the wavelength dependence of the radiance distribution parameter $E_u(\lambda, 0-)/L_u(\lambda, 0-)$ is typically taken to be spectrally quite flat, it apparently becomes more variable for $\lambda < 440$ nm and $\lambda > 550$ nm [*Austin*, 1979; *R. Smith*, unpublished Sargasso Sea data, 1991; *C. Davis*, unpublished California Current data, 1991]. This problem cannot be so easily ignored.

In addition, recent measurements and model results indicate that for oligotrophic environments, Raman inelastic scattering is not negligible [*Marshall and Smith*, 1990; *Stavn*, 1990; *Peacock et al.*, 1990] and that for CDOM-rich environments, solar stimulated fluorescence of the CDOM may likewise not be negligible [*Hawes and Carder*, 1990; *Peacock et al.*, 1990]. Contributions to the photon flux by these source-like phenomena will exert a maximum effect in the blue-green wavelengths near the sea surface where UV and near-UV light is available to stimulate emission of blue and green photons. This is so because both the Raman scattering cross section and CDOM absorption increase with decreasing wavelength and because the availability of UV light for excitation decreases rapidly with depth.

An understanding of the effects of these transpectral

phenomena on spectral ratios of $L_w(\lambda)$ is necessary in order to modify the model and algorithm appropriately for use with satellite-derived $L_w(\lambda)$ data. *Peacock et al.* [1990] estimated these effects to be of second-order importance, affecting $L_w(\lambda)$ by less than 15%. If this is indeed the case, the modifications necessary should not be major.

5.6. Conclusion

For the California Current region where $[\text{Chl } a] \leq 1.3$ mg m^{-3} , the confounding effects of absorption due to primary productivity degradation products on remote assessment of chlorophyll *a* can be removed to a large extent by the addition of a blue spectral channel at about 412 nm to the nominal suite of CZCS-like channels expected on SeaWiFS and other future ocean color scanners. It is anticipated that DP models such as the one described here will be somewhat site- and perhaps season-specific and that they will significantly enhance the accuracy of remotely sensed estimates of $[\text{Chl } a]$ for waters rich in marine productivity degradation products. A noteworthy feature of the DP-model is that the individual absorption and scattering parameters can be customized for a given province. A particularly important task is to develop empirical descriptions of the variation in $a^*_\phi(\lambda)$ with respect to $[\text{Chl } a]$, which is due primarily to variations in phytoplankton species composition and light- and nutrient-histories. Presently, the technique best suited to determine these relationships is the improved quantitative filter technique of *Mitchell* [1990], augmented by both the detrital correction method of *Kishino et al.* [1985] and the pheopigment absorption correction of *Roessler et al.* [1989].

NOTATION

λ	wavelength of light, nm.
$a_x(\lambda)$	absorption coefficient for any component x , at wavelength λ , m^{-1} (subscripts ϕ , cdom, dp, f , h , p , pdp, and w refer to phytoplankton, CDOM, DP, MFA, MHA, particles, PDP, and water).
$a^*_x(\lambda)$	mass-specific absorption coefficient for any component x at wavelength λ , $\text{m}^2 \text{g}^{-1}$ (subscripts described above).
$a^*_\phi(\lambda), a^*_p(\lambda)$	Chl <i>a</i> -specific absorption coefficients for phytoplankton and particles at wavelength λ , $\text{m}^2 [\text{mg Chl } a]^{-1}$.
$b'_p(\lambda), b'_w(\lambda)$	backscattering coefficients for particles and water at wavelength λ , m^{-1} .
$[C]$	concentration of chlorophyll <i>a</i> + pheophytin <i>a</i> , mg m^{-3} .
C_x	concentration of component x , g m^{-3} (subscripts described above).
C'_{dp}, C'_h	weighted concentration parameter for DP and MHA, g m^{-3} (the prime indicates that the values are weighted by the presence of PDP via the specific absorption coefficients (see equation (15)).
$\text{DOC}_{\text{pt}}, \text{DOC}_{\text{uv}}$	dissolved organic carbon, as determined by the platinum catalyst method and by the ultraviolet oxidation method, g m^{-3} .
$E_d(\lambda, z), E_u(\lambda, z)$	downwelling and upwelling irradiances at wavelength λ and depth z , $\text{W m}^{-2} \text{nm}^{-1}$.

- f' fulvic acid fraction of DP (the prime indicates that the fraction is weighted by the presence of PDP via the specific absorption coefficients (see equations (15) and (17)).
- $k_d(490)$ diffuse attenuation coefficient for downwelling irradiance at 490 nm, m^{-1} .
- $L_u(\lambda)$ subsurface upwelling radiance at wavelength λ , $W\ m^{-2}\ sr^{-1}\ nm^{-1}$.
- $L_w(\lambda)$ water-leaving radiance at wavelength λ , $W\ m^{-2}\ sr^{-1}\ nm^{-1}$.
- n number of samples.
- r_{ij} ratio of water-leaving radiances at wavelengths λ_i and λ_j .
- r^2 correlation coefficient of regression.
- $R(\lambda)$ irradiance reflectance at wavelength λ .
- $R_{rs}(\lambda)$ remote sensing reflectance at wavelength λ .
- S_x spectral slopes for the exponential expressions that describe absorption due any component x , nm^{-1} (subscripts f , h , and pdp refer to MFA, MHA, and PDP).
- z depth, m.

Acknowledgments. This study was supported by NASA grants NAGW-465 and NAS5-30779 and ONR grant N00014-89-J-1091. We also acknowledge ONR for funding the Optical Dynamics Experiment which provided the data used in the algorithm development.

REFERENCES

- Abbott, M. R., K. H. Brink, C. R. Booth, D. Blasco, L. A. Codispoti, P. P. Niiler, and S. R. Ramp, Observations of phytoplankton and nutrients from a Lagrangian drifter off northern California, *J. Geophys. Res.*, **95**, 9393-9409, 1990.
- Altabet, M. A., Organic C, N, and stable isotope composition of particulate matter collected on glass-fiber and aluminum oxide filters, *Limnol. Oceanogr.*, **35**, 902-909, 1990.
- Armstrong, F. A., P. M. Williams, and J. D. Strickland, Photo-oxidation of organic matter in seawater by ultra-violet radiation: Analytical and other applications, *Nature*, **211**, 481-483, 1966.
- Austin, R. W., Inherent spectral radiance signatures of the ocean surface, in *Ocean Color Analysis, SIO Ref. 74-10*, pp. 2.1-2.20, Scripps Inst. of Oceanogr., La Jolla, Calif., 1974.
- Austin, R. W., Coastal zone color scanner radiometry, in *Ocean Optics VI, Proc. Soc. Photo Opt. Instrum. Eng.*, **208**, 170-177, 1979.
- Baker, K. S., and R. C. Smith, Bio-optical classification and model of natural waters 2, *Limnol. Oceanogr.*, **27**, 500-509, 1982.
- Bird, R. E., and C. Riordan, Simple solar spectral model for direct and diffuse irradiance on horizontal and tilted planes at the earth's surface for cloudless atmospheres, *J. Clim. Appl. Meteorol.*, **25**, 87-97, 1986.
- Bricaud, A., A. Morel, and L. Prieur, Absorption by dissolved organic matter in the sea (yellow substance) in the UV and visible domains, *Limnol. Oceanogr.*, **26**, 43-53, 1981.
- Bricaud, A., A. Morel, and L. Prieur, Optical efficiency factors of some phytoplankters, *Limnol. Oceanogr.*, **28**, 816-832, 1983.
- Bricaud, A., A.-L. Bedhomme, and A. Morel, Optical properties of diverse phytoplanktonic species: Experimental results and theoretical interpretation, *J. Plankton Res.*, **10**, 851-873, 1988.
- Carder, K. L., and R. G. Steward, A remote-sensing reflectance model of a red-tide dinoflagellate off west Florida, *Limnol. Oceanogr.*, **30**, 286-298, 1985.
- Carder, K. L., R. G. Steward, J. H. Paul, and G. A. Vargo, Relationships between chlorophyll and ocean color constituents as they affect remote-sensing reflectance models, *Limnol. Oceanogr.*, **31**, 403-413, 1986.
- Carder, K. L., R. G. Steward, G. R. Harvey, and P. B. Ortner, Marine humic and fulvic acids: Their effect on remote sensing of ocean chlorophyll, *Limnol. Oceanogr.*, **34**, 68-81, 1989.
- Clarke, G. L., G. C. Ewing, and C. J. Lorenzen, Spectra of backscattered light from the sea obtained from aircraft as a measure of chlorophyll concentration, *Science*, **167**, 1119-1121, 1970.
- Druffel, E. R. M., P. M. Williams, and Y. Suzuki, Concentrations and radiocarbon signatures of dissolved organic matter in the Pacific Ocean, *Geophys. Res. Lett.*, **16**(9), 991-994, 1989.
- Dubinsky, Z., P. G. Falkowski, and K. Wyman, Light harvesting and utilization by phytoplankton, *Plant Cell Physiol.*, **27**, 1335-1349, 1986.
- Frouin, R., D. W. Linger, C. Gautier, K. A. Baker, and R. C. Smith, A simple analytical formula to compute clear sky total and photosynthetically available solar irradiance at the ocean surface, *J. Geophys. Res.*, **94**, 9731-9742, 1989.
- Gordon, H. R., Ship perturbation of irradiance measurements at sea, 1, Monte Carlo simulations, *Appl. Opt.*, **23**, 4172-4182, 1985.
- Gordon, H. R., and A. Y. Morel, *Remote Assessment of Ocean Color for Interpretation of Satellite Visible Imagery: A Review*, Springer-Verlag, New York, 1983.
- Gordon, H. R., O. B. Brown, and M. M. Jacobs, Computed relationships between the inherent and apparent optical properties of a flat homogeneous ocean, *Appl. Opt.*, **14**, 417-427, 1975.
- Gordon, H. R., D. K. Clark, J. W. Brown, O. B. Brown, R. H. Evans, and W. W. Broenkow, Phytoplankton pigment concentrations in the Middle Atlantic Bight: Comparison of ship determinations and CZCS estimates, *Appl. Opt.*, **22**, 20-36, 1983.
- Gordon, H. R., O. B. Brown, R. H. Evans, J. W. Brown, R. C. Smith, K. S. Baker, and D. K. Clark, A semianalytical model of ocean color, *J. Geophys. Res.*, **93**, 10,909-10,924, 1988.
- Gregg, W. W., and K. L. Carder, A simple 1 nm resolution solar irradiance model for cloudless maritime atmospheres, *Limnol. Oceanogr.*, **35**, 1657-1675, 1990.
- Harvey, G. R., D. A. Boran, L. A. Chesal, and J. M. Tokar, The structure of marine fulvic and humic acids, *Mar. Chem.*, **12**, 119-132, 1983.
- Hawes, S. K., and K. L. Carder, Fluorescence quantum yields of marine humic and fulvic acids: Application for in situ determination, *Eos Trans. AGU*, **71**(2), 136, 1990.
- Hayase, K., and H. Tsubota, Sedimentary humic acid and fulvic acid as fluorescent organic materials, *Geochem. Cosmochim. Acta*, **49**, 159-163, 1985.
- Herbland, A., A. Le Bouteiller, and R. Raimbault, Size structure of phytoplankton biomass in the equatorial Atlantic Ocean, *Deep Sea Res.*, **32**, 819-836, 1985.
- Hojerslev, N. K., Inherent and apparent optical properties of the Baltic, *Rep. 23*, Inst. of Phys. Oceanogr., Univ. of Copenhagen, 1974.
- James, H. R., and E. A. Birge, A laboratory study of the absorption of light by lake waters, *Trans. Wis. Acad. Sci. Arts Lett.*, **31**, 1-154, 1938.
- Jeffrey, S. W., Algal pigment systems, in *Primary Productivity in the Sea, Brookhaven Symp. Biol.*, **31**, 33-58, 1980.
- Jerlov, N. G., Factors influencing the transparency of the Baltic waters, *Medd. Oceanogr. Inst. Goteborg*, **25**, 1955.
- Justus, C. G., and M. V. Paris, A model for solar spectral irradiance and radiance at the bottom and top of a cloudless atmosphere, *J. Clim. Appl. Meteorol.*, **24**, 193-205, 1985.
- Kalle, K., What do we know about the "Gelbstoff"? *Monogr.*, **10**, pp. 59-62, International Union of Geophysics and Geology, 1961.
- Kalle, K., The problem of Gelbstoff in the sea, *Oceanogr. Mar. Biol.*, **4**, 91-104, 1966.
- Kiefer, D. A., and B. G. Mitchell, A simple, steady state description of phytoplankton growth based on absorption cross section and quantum efficiency, *Limnol. Oceanogr.*, **28**, 770-776, 1983.
- Kiefer, D. A., and J. B. Soohoo, Spectral absorption by marine particles of coastal waters of Baja California, *Limnol. Oceanogr.*, **27**, 492-499, 1982.
- Kirk, J. T. O., Yellow substance (gelbstoff) and its contribution to the attenuation of photosynthetically active radiation in some inland and coastal southeastern Australian waters, *Aust. J. Mar. Freshwater Res.*, **27**, 61-71, 1976.
- Kirk, J. T. O., Spectral absorption properties of natural waters: Contribution of the soluble and particulate fractions to light absorption in some inland waters of southeastern Australia, *Aust. J. Mar. Freshwater Res.*, **31**, 287-296, 1980.

- Kirk, J. T. O., *Light and Photosynthesis in Aquatic Ecosystems*, Cambridge University Press, New York, 1983.
- Kirk, J. T. O., Dependence of relationship between inherent and apparent optical properties of water on solar altitude, *Limnol. Oceanogr.*, 29, 350–356, 1984.
- Kishino, M., M. Takahashi, N. Okami, and S. Ichimura, Estimation of the spectral absorption coefficients of phytoplankton in the sea, *Bull. Mar. Sci.*, 37, 634–642, 1985.
- Laws, E. A., G. R. DiTullio, K. L. Carder, P. R. Betzer, and S. K. Hawes, Primary production in the deep blue sea, *Deep Sea Res.*, 37, 715–730, 1990.
- Lundgren, B., Spectral transmittance measurements in the Baltic, *Rep. 30*, Inst. of Phys. Oceanogr., Univ. of Copenhagen, 1976.
- Marshall, B. R., and R. C. Smith, Raman scattering and in-water ocean optical properties, *Appl. Opt.*, 29, 71–84, 1990.
- Mitchell, B. G., Algorithms for determining the absorption coefficients for aquatic particulates using the Quantitative Filter Technique, in Ocean Optics X, *Proc. SPIE Int. Soc. Opt. Eng.*, 1302, 137–148, 1990.
- Mitchell, B. G., Predictive bio-optical relationships for polar oceans and marginal ice zones, *J. Mar. Syst.*, in press, 1991.
- Mitchell, B. G., and O. Holm-Hansen, Bio-optical properties of Antarctic waters: Differentiation from temperate ocean models, *Deep Sea Res.*, 38(8–9), 1009–1028, 1991.
- Mitchell, B. G., and D. A. Kiefer, Determination of absorption and fluorescence excitation spectra for phytoplankton, in *Marine Phytoplankton and Productivity*, edited by O. Holm-Hansen et al., pp. 157–169, Springer-Verlag, New York, 1984.
- Mitchell, B. G., and D. A. Kiefer, Chlorophyll *a* specific absorption and fluorescence excitation spectra for light-limited phytoplankton, *Deep Sea Res.*, 35, 639–663, 1988a.
- Mitchell, B. G., and D. A. Kiefer, Variability in pigment specific particulate fluorescence and absorption spectra in the northeastern Pacific Ocean, *Deep Sea Res.*, 35, 665–689, 1988b.
- Morel, A. Y., Optical properties of pure water and sea water, in *Optical Aspects of Oceanography*, edited by N. G. Jerlov and E. Steeman Nielsen, pp. 1–24, Academic, San Diego, Calif., 1974.
- Morel, A. Y., In-water and remote measurement of ocean color, *Boundary Layer Meteorol.*, 18, 177–201, 1980.
- Morel, A. Y., Optical modeling of the upper ocean in relation to its biogenous matter content (case I waters), *J. Geophys. Res.*, 93, 10,749–10,768, 1988.
- Morel, A. Y., and A. Bricaud, Theoretical results concerning light absorption in a discrete medium and application to the specific absorption of phytoplankton, *Deep Sea Res.*, 28, 1357–1393, 1981.
- Morel, A. Y., and H. R. Gordon, Report of the working group on ocean color, *Boundary Layer Meteorol.*, 18, 343–355, 1980.
- Morel, A. Y., and L. Prieur, Analysis of variations in ocean color, *Limnol. Oceanogr.*, 22, 709–722, 1977.
- Mueller, J. L., and R. E. Lange, Bio-optical provinces of the northeast Pacific Ocean: A provisional analysis, *Limnol. Oceanogr.*, 34, 1572–1586, 1989.
- Peacock, T. P., K. L. Carder, and R. G. Steward, Components of spectral attenuation for an offshore jet in the Coastal Transition Zone, *Eos Trans. AGU*, 69, 1125, 1988.
- Peacock, T. P., K. L. Carder, C. O. Davis, and R. G. Steward, Effects of fluorescence and water Raman scattering on models of remote sensing reflectance, in Ocean Optics X, *Proc. SPIE Int. Soc. Opt. Eng.*, 1302, 303–319, 1990.
- Platt, T., Primary production of the ocean water column as a function of surface light intensity: Algorithm for remote sensing, *Deep Sea Res.*, 33, 149–163, 1986.
- Platt, T., and S. Sathyendranath, Oceanic primary production: estimation by remote sensing at local and regional scales, *Science*, 241, 1613–1620, 1988.
- Prieur, L., and S. Sathyendranath, An optical classification of coastal and oceanic waters based on the specific spectral absorption curves of phytoplankton pigments, dissolved organic matter, and other particulate materials, *Limnol. Oceanogr.*, 26, 671–689, 1981.
- Roesler, C. S., M. J. Perry, and K. L. Carder, Modeling in situ phytoplankton absorption from total absorption spectra in productive inland marine waters, *Limnol. Oceanogr.*, 34, 1510–1523, 1989.
- Smith, R. C., and K. S. Baker, Optical classification of natural waters, *Limnol. Oceanogr.*, 23, 260–267, 1978.
- Smith, R. C., and K. S. Baker, Optical properties of the clearest natural waters (200–800 nm), *Appl. Opt.*, 20, 177–184, 1981.
- Smith, R. C., and K. S. Baker, Oceanic chlorophyll concentrations as determined by satellite (Nimbus-7 coastal zone color scanner), *Mar. Biol.*, 66, 269–279, 1982.
- Smith, R. C., and K. S. Baker, The analysis of ocean optical data, in Ocean Optics VII, *Proc. SPIE Int. Soc. Opt. Eng.*, 489, 119–126, 1984.
- Smith, R. C., and K. S. Baker, The analysis of ocean optical data, 2, in Ocean Optics VIII, *Proc. SPIE Int. Soc. Opt. Eng.*, 637, 95–107, 1986.
- Smith, R. C., and W. H. Wilson, Ship and satellite bio-optical research in the Southern California Bight, in *Oceanography From Space*, edited by J. F. Gower, pp. 281–294, Plenum, New York, 1981.
- Smith, R. C., K. S. Baker, and P. Dunstan, Fluorometric techniques for the measurement of oceanic chlorophyll in the support of remote sensing, *SIO Ref. 81-17*, 14 pp., Scripps Inst. of Oceanogr., La Jolla, Calif., 1981.
- Smith, R. C., C. R. Booth, and J. Starr, Oceanographic bio-optical profiling system, *Appl. Opt.*, 23, 2791–2797, 1984.
- Smith, R. C., B. B. Prezelin, R. R. Bidigare, and K. S. Baker, Bio-optical modeling of photosynthetic production in coastal waters, *Limnol. Oceanogr.*, 34, 1524–1544, 1989.
- Sosik, H., and B. G. Mitchell, Absorption, fluorescence, and quantum yield for growth in nitrogen-limited *Dunaliella tertiolecta*, *Limnol. Oceanogr.*, 36, 910–921, 1991.
- Stavn, R. H., Raman scattering effects at the shorter visible wavelengths in clear ocean waters, in Ocean Optics X, *Proc. SPIE Int. Soc. Opt. Eng.*, 1302, 94–100, 1990.
- Stramski, D., Artifacts in measuring absorption spectra of phytoplankton collected on a filter, *Limnol. Oceanogr.*, 35, 1804–1809, 1990.
- Stuermer, R. H., The characterization of humic substances in sea water, Ph.D. thesis, Mass. Inst. of Technol./Woods Hole Oceanogr. Inst., Woods Hole, Mass., 1975.
- Sugimura, T., and Y. Suzuki, A high temperature catalytic oxidation method for non-volatile dissolved organic carbon in seawater by direct injection of liquid samples, *Mar. Chem.*, 42, 105–131, 1988.
- Suzuki, Y., T. Sugimura, and T. Itoh, A catalytic oxidation method for determination of total nitrogen dissolved in seawater, *Mar. Chem.*, 16, 83–97, 1985.
- Topliss, B. J., J. R. Miller, and B. Irwin, Ocean optical measurements, I, Statistical analysis of data from the western North Atlantic, *Cont. Shelf Res.*, 9(2), 113–131, 1989.
- K. A. Baker, Marine Bio-Optics, Scripps Institution of Oceanography, A-018, University of California, San Diego, La Jolla, CA 92093.
- K. L. Carder, S. K. Hawes, and R. G. Steward, Marine Science Department, University of South Florida, 140 Seventh Avenue South, St. Petersburg, FL 33701.
- B. G. Mitchell, Ocean Productivity Program, NASA, Mail Code SEL, Room 209, Washington, DC 20546.
- R. C. Smith, Center for Remote Sensing and Environmental Optics, University of California, Santa Barbara, CA 93106.

(Received March 1, 1991;
 revised July 8, 1991;
 accepted August 13, 1991.)